JCTC Journal of Chemical Theory and Computation

Article

pubs.acs.org/JCTC

Modeling the Self-Assembly of Nano Objects: Applications to Supramolecular Organic Monolayers Adsorbed on Metal Surfaces

Thomas J. Roussel*,† and Lourdes F. Vega‡

†Institut de Ciència de Materials de Barcelona, Consejo Superior de Investigaciones Científicas (ICMAB-CSIC), Campus de la UAB, 08193 Bellaterra, Spain

‡MATGAS Research Center (Carburos Metálicos/Air Products, CSIC, UAB), Campus de la UAB, 08193 Bellaterra, Spain

Supporting Information

ABSTRACT: We present here the implementation of a code developed for the simulation of the self-assembly of nano objects (SANO). The code has the ability to predict the molecular self-assembly of different structural motifs by tuning the molecular building blocks as well as the metallic substrate. It consists in a two-dimensional grand canonical Monte Carlo (GCMC) approach developed to perform atomistic simulations of thousands of large organic molecules self-assembling on metal surfaces. By computing adsorption isotherms at room temperature and spanning over the characteristic submicrometric scales, we confront the robustness of the approach with three different well-known systems: $ZnPcCl_8$ on Ag(111), $CuPcF_{16}$ on Au(111), and PTBC on Ag(111). We retrieve respectively their square, oblique, and hexagonal supramolecular tilling. The code incorporates generalized force fields to describe the molecular interactions, which provides transferability to many organic building blocks and metal surfaces. Ultimately, the method is versatile and can be an interesting multiscale approach if one aims to bridge quantum level calculations to the experimental scales and within a treatment in temperature.

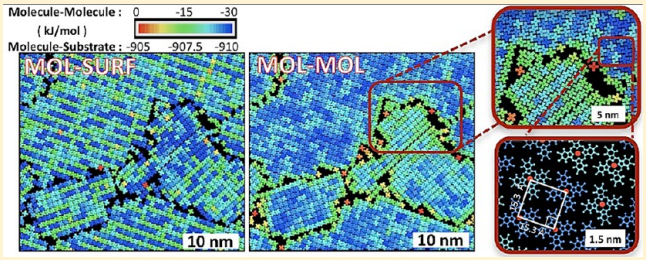

1. INTRODUCTION

Toward the tailoring of new functional materials, the development of new methods to model and predict the self-assembly of organic molecules adsorbed on surfaces is crucial. A deep knowledge of the optimal conditions to precisely steer and monitor the first molecular building blocks is fundamental for metal-driven molecular architectonic.[1,2] The heteroepitaxial properties determine their structural and physical properties and can be tuned by choosing adequately the molecular building blocks and the substrate. The symmetry and periodicity of the organic layer can be adjusted by modifying the chemistry of the molecular building block[3] or by using molecular templates[4] and reconstructed surfaces.[5] Besides, multicomponent architectures stem from molecular codeposition open a wide range of tunable physical properties, which are dependent on the composition.[6]

The basic principles behind the molecular self-assembly of organic molecules on metal surfaces and their epitaxial organization on solid substrates are well understood.[7,8] Modeling based on quantum mechanics (QM) and the density functional theory (DFT) is widely used to bring a deep understanding of the optical and electronic properties of these new materials and the change of the work function[9] or to provide interpretations of the experimental images obtained by scanning tunneling microscopy (STM).[10] However, these simulations are limited to few hundreds of atoms and are not suitable to render the thermodynamics properties and the collective process of the molecular self-ordering. Conversely, classical approaches can compute thousands of atoms providing insights on supramolecular self-assembly. For instance, we could perform molecular dynamics (MD) simulations with more than 3×10^4 atoms to model shiff-based macrocycle molecules self-assembled on gold surface with an explicit organic solvent.[11] Nevertheless, this approach is computationally limited in time scale since it encompasses few nanoseconds, while supramolecular self-orderings occur on large domains and for longer time scale (from few minutes to hours).[12] It implies the modeling of thousands of large molecules if one aims to describe the subtle and competitive interplay between the intermolecular and the interfacial interactions. The Monte Carlo (MC) method is a more suitable approach to avoid this time scale limitation, but it still suffers of the large number of degrees of freedom. Different strategies can be found in the literature to overcome these limitations. Among them, the kinetic Monte Carlo (kMC)[13] is employed to simulate the first steps of growth during the deposition by molecular beam epitaxy. Assuming that the metallic substrate role is only to constrain the molecular system in two dimensions, Weber et al.[14] could build the structural stabilities diagram with temperature versus the molecular coupling anisotropy and predict the occurrence of open networks, compact phases, and disordered phases. Silly et al. could also derive the hydrogen binding energies as a function of the molecular mixture

Received: December 23, 2012
Published: April 5, 2013

stoichiometry, combining this latter approach with an empirical description of the intermolecular interactions.[15] However, the lattice MC imposes to the molecules an already defined symmetry and positions, which deprives the organic layer to adjust its epitaxial properties and to release the accumulated stress due to the mismatch with the surface. Interestingly, two-dimensional (2D) off-lattice strategies were recently proposed, describing the molecular building block in a coarse-grained manner. For instance, Patti et al. have modeled successfully the self-assembling behavior of amphiphilic cyclodextrins represented in their essential and most characteristic picture.[16] Nevertheless, this approach looses the atomistic details of the molecules and is not easily transferable to other molecules. Fortuna et al. have proposed the combination of MC/MD of rigid molecules taking advantage of the agent-based (AB) algorithm to study the self-assembly of a fully atomistic model.[17−19] They have shown that AB/MC gives lower configuration energies in the same simulation time than both MC and MD simulation techniques and the most conventional simulated annealing MC[20] method. However, the biased AB/MC technique suffers of not respecting the detailed balance.

Therefore, atomistic simulations of thousands of large organic molecules remain challenging and require computational efforts that become rapidly unaffordable when the number of atoms per molecule is large. To overcome this limitation, one freezes the intramolecular degrees of freedom of the molecules and the substrate, assuming that they play a minor role on the self-ordering. It allows the implementation of grid interpolation technique that reduces dramatically the computational time consumption. Precalculation of the interactions between the adsorbate and the adsorbent is commonly used to model gas adsorption isotherms[21,22] or, for instance, to determine the zeolite templated carbon nanostructures.[23] By extending the grid interpolation technique to the interactions between molecules, Mannsfeld et al. could study the heteroepitaxial properties of highly ordered organic monolayer. They have performed simulated annealing temperature MC[24] with initial configurations involving thousands of molecules already highly ordered.[25,26] We propose here a predictive numerical tool extending the latter technique to the grand ensemble in order to start from the bare metal surface and simulate the entire molecular self-ordering. For that, we have implemented and performed a 2D grand canonical Monte Carlo approach (GCMC),[27] which consists in minimizing the configurational energy, while it maximizes the entropy within fixed chemical potential (μ) and temperature.

We will first present the methodology implemented in the self-assembly of nano-object code (SANO) and further discuss the results obtained for three different systems. First on the adsorption of octachloro-zinc-phthalocyanines ($ZnPcCl_8$) on dense silver surface $Ag_{(111)}$. We analyze the domain-size distribution as a function of the chemical potential to illustrate the ordering behavior during the adsorption isotherms. To demonstrate the transferability of the approach, we discuss the results obtained for two other model systems: the adsorption of copper-phthalocyanines-fluorinated ($CuPcF_{16}$) on gold surface and the adsorption of penta-*tert*-butylcorannulene (PTBC) on silver $Ag_{(111)}$. The former molecule has been reported to adopt an oblique structure on copper and gold surface[28] and, more interestingly, to form long-range ordered bicomponent layers when it is coadsorbed with di-indenoperylene (DIP).[29,30] On the other hand, the PTBC molecule was shown to form long-range hexagonal order despite of its five-fold symmetry and to lead to a large diversity of ordered phases when coadsorbed with $ZnPcCl_8$ on $Ag_{(111)}$.[31]

2. SANO GRID METHODOLOGY

2.1. Grid Interpolation Scheme. Submicrometric scale simulations imply thousands of organic building blocks, which become computationally very demanding when the number of atom per molecule is large. The grid interpolation technique, first implemented by Mannsfeld et al.,[26,32] enables the calculation of both molecule−substrate and molecule−molecule interactions in a very fast way (see Figure 1). It assumes

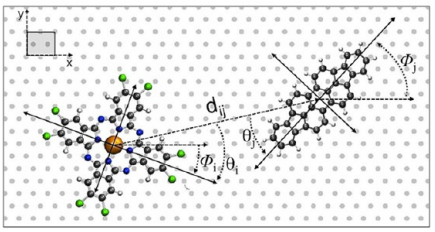

Figure 1. Scheme of the grid interpolation technique for the intermolecular potential energy between a $ZnPcCl_8$ and DIP.

the internal degrees of freedom frozen for both the substrate and the molecular building blocks. Therefore, it allows precalculations of the potential energy between two building blocks and the building block with one unit cell of the surface.

The total potential energy of the system is expressed through two main contributions, the molecule−molecule interactions (V^{MM}) and molecule−substrate interaction (V^{MS}) as follows:

$$E_{tot} = \sum_{I=1}^{Nmol} \sum_{J\neq I}^{Nmol} (V^{MM}(\theta_I, \theta_J, d_{IJ}) + V^{MS}(x_r^I, y_r^I, \theta_I)) \quad (1)$$

where x_r^i and y_r^i are the reduced coordinates of the molecular center of mass (COM) position (of the molecule indexed i) folded in the orthogonal unit cell of the metal surface, and the intermolecular distance (d_{ij}) between the pairs of molecules i and j their respective COM, their reduced position and the two algebraic angles (θ_i and θ_j) relatively to the axis $\mathbf{d}_{ij}$, respectively extracted during the simulations from their two azimuthal molecular orientations (ϕ_i and ϕ_j).

Once the potential energy precalculation is achieved and stored, the computational time to evaluate the potential energy is not anymore a function of the number of atoms per molecule but only of the number of molecules. Therefore, it reduces dramatically the computational time and allows performing full MC calculations. Three preliminary steps are necessary before performing the GCMC simulation: (i) the optimization of the organic molecule atomic structure and the determination of the partial charge distribution generally provided by sophisticated QM and DFT approaches (i.e., Hyperchem[33] or Siesta[34] codes); (ii) independently, we build a realistic surface of the metal structure and propose in this work the use of a quench MD to simulate large metal structures. The choice of the model will be discussed in details later. (iii) From the two previous steps, we precalculate and store separately the molecule surface and the intermolecular potential energies. We discuss now in more detail each of these steps.

2.1.1. Precalculation of the Interfacial Interactions. We perform a minimization of the potential energy V^{MS} dividing

dx.doi.org/10.1021/ct3011248 | J. Chem. Theory Comput. 2013, 9, 2161−2169

one orthorhombic unit cell of the surface in (50 × 50) points and for the 360 orientations possible of the molecule. We store the V^{MS} in a (50 × 50 × 360) matrix for each azimuthal distance (z_o) between the molecule and the surface that minimizes the potential energy. Note that the variation of z_o is <0.1 Å. The potential energy V^{MS} is declined in two contributions: a van der Waals contribution (represented by a 12-6 LJ potential) and a Coulomb contribution to the binding strength corresponding to the induced polarization of the metal surface represented by an attractive image potential of the partial charges carried by the molecule.[35−37]

$$V^{MS}(x_r^I, y_r^I, \phi_I)_{z_o} = \sum_{i=1}^{N_{atom}^{molecule}} \sum_{j=1}^{M_{atom}^{metal}} \left(4\varepsilon_{ij} \underbrace{\left[\left(\frac{\sigma_{ij}}{r_{ij}}\right)^{12} - \left(\frac{\sigma_{ij}}{r_{ij}}\right)^{6} \right]}_{\text{OPLS-AA}} \right)_{z_o} + \left(\frac{1}{4\pi\varepsilon} \sum_{i=1}^{N_{charges}} \left[\frac{-q_i^2}{2|z_i - z_M|} + \sum_{j\neq 1}^{N_{charges}} \frac{-q_i q_j}{\sqrt{(x_j - x)^2 + (y_j - y_i)^2 + (z_i + z_j - 2z_M)}} \right] \right)_{z_o} \quad (2)$$

where the first summation provides the LJ contribution over the N atoms of the molecule and the M atoms of the surface with a cutoff range of 25 Å. The parameters (σ and ε) for the metal atoms are those reported by Heinz et al.[38] for several (*fcc*) transition metals (Ag, Al, Au, Cu, Ni, Pb, Pd, Pt) and their different facets {*h*,*k*,*l*}.[39] They reproduce accurately the quantitative and qualitative experimental surface tensions and interfacial properties of water molecules and organic molecules adsorbed on metal surfaces under ambient conditions. The atomic parameters for the organic molecules are taken from the OPLS all-atom force field (OPLS-AA) parameters.[40] The geometric mixing rule is applied to define the crossed parameters.

The second summation over the N partial charges localized on the atomic nuclei of the molecule and the N mirror charges. It reflects the polarization of the surface through the image potential of the charges carried by the molecule itself and for a fixed location of the image plane located at the jellium edge z_M from the first layer of the metal surface.[41] The image potential from the molecule itself represents <2.5% of the total molecule-surface potential energy (i.e., −6 kcal/mol among the −220 kcal/mol in the case of $ZnPcCl_8$ adsorbed on $Ag_{(111)}$). It mainly contributes in the surface-imposed orientation of the molecule. The contribution of the image potential due to the presence of neighboring molecules should be also included, moreover if the molecules are charged or in presence of a polar solvent.[37] However, for the three systems we have been studying, it appears to contribute <0.001% to the minimum of potential energy. Therefore, we neglect it to perform the MC simulation efficiently. It is worthy to point out that the LJ parameters implicitly reproduce the essential features of the electronic metal structure, so that computed interfacial energies for flat surfaces are of the same accuracy as a tight binding or DFT methods, or quantum mechanical methods.[38,42] A major benefit is that computation times are about 10^6 times shorter compared to ab initio methods. This latter important attribute allows the precalculation of the molecule-surface potential energy (V^{MS}) even if the surface has a large unit cell, for instance, if we consider defects, vicinal or reconstructed surfaces. Note that the SANO code is also implemented with CHARMM parameters,[43] however, herein, we only discuss results obtained with the OPLS-AA force field.

2.1.2. Precalculation of the Intermolecular Interactions. In this work, the intermolecular weak interactions are described with dispersive (LJ) and Coulombic terms. For an issue of computational efficiency, the latter is evaluated only in its real part being aware that the total charge of each molecule is neutral and the multipolar contribution will not diverge depending on the cutoff choice. The cutoff range is taken large enough (e.g., 3−5 nm) to ensure 99% of its contribution between two molecules. The intermolecular interactions when performing MC simulations are equivalent to the following atomistic calculation:

$$V^{MM}(\theta_I, \theta_J, d_{IJ}) = \sum_{i=1}^{N_{atom}^{moleculeI}} \sum_{j=1}^{N'^{atom}_{moleculeJ}} \left(4\varepsilon_{ij} \underbrace{\left[\left(\frac{\sigma_{ij}}{r_{ij}}\right)^{12} - \left(\frac{\sigma_{ij}}{r_{ij}}\right)^{6} \right]}_{\text{OPLS-AA}} \right) + \sum_{i=1}^{N_{charges}^{moleculeI}} \sum_{j=1}^{N'^{charges}_{moleculeJ}} \left(\frac{1}{4\pi\varepsilon} \left[\frac{q_i q_j}{r_{ij}} \right] \right) \quad (3)$$

where i and j are respectively the i^{th} and j^{th} atom of the molecule indexed I and J, and q their corresponding charges. The dielectric constant is taken to one. We calculate (360 × 360 × 200) grid points corresponding to each 360 azimuthal orientations of both molecules and 200 intermolecular distances between the minimum and maximum cutoff distances (respectively 10 and 30 Å). Note that the SANO code is also implemented for bimolecular self-ordering. Therefore, three grids would be necessary to simulate the coadsorption processes. It is worthy to point out here that once the precalculation is achieved, the SANO code will perform with the same efficiency the MC calculations independently of the number of atoms per molecule.

2.2. Generating a Realistic Transition-Metal Surface. We generate the metal structures along the (111) orientation of the crystalline face-centered cubic (*fcc*) structure. We build slab structures made of 12 dense layers stacked along *z*-axis and perform a quenched MD[27,44] to relax the surface of the metal. The covalent bonds between the metal atoms are described by a semiempirical many-body potential derived from the tight binding scheme proposed by Ducastelle[45] in its second moment approximation (TB-SMA).[46]

Gupta[47] has reported that the choice of a based-on Friedel's thigh binding model yields physical contraction of *fcc* (100), (110), and (111) surfaces, proper to the square root function of the atomic coordination number. Additionally, they have demonstrated that a simple pairwise potential yields intrinsically to a nonphysical expansion of the interlayer distances at the metal surface. This latter unrealistic expansion would prejudice the adsorption potential energy calculation.

The total energy of a system of N atoms is then written as

$$E_{cohesion} = \sum_{i}^{N_{at}} \left(\sqrt{\sum_{j\neq i}^{N_{at}} \xi^2 \left(-\exp^{2q\left(\frac{r_{ij}}{r_o} - 1\right)} \right)} + A \exp^{p\left(\frac{r_{ij}}{r_o} - 1\right)} \right) \quad (4)$$

dx.doi.org/10.1021/ct3011248 | J. Chem. Theory Comput. 2013, 9, 2161−2169

where ξ in the attractive term is an effective hopping integral, summed over all the interatomic distances r_{ij} (when $r_{ij} < r_c$) for a pair of atoms at sites i and j. The set of parameters (A, ξ, p, q) are adjusted on the bulk modulus, elastic constants, and cohesive energies. It renders accurately bulk and surface properties, for instance, for silver transition metal,[48,49] and the interfacial properties of epitaxial silver clusters deposited on $MgO_{(100)}$ oxide.[50] Among others, we provide in the Supporting Information (SI) different sets of parameters for the transition metals considered in this work and exhaustive references for other metal parameters. Note that a whole set of parameters has been reported recently to adjust bulk, elastic, and surface energies properties at a time.[51]

2.3. The 2D GCMC Approach. We have implemented a standard 2D GCMC simulations, which advantageously insures the detailed balance. [52] We perform at least 10^6 MC attempts per molecule to reach equilibrium. The attempts are either an insertion at a random place of a molecule or a molecule is picked at random and then either extracted, translated, rotated, or translated and rotated at a time. The decision whether to translate or reorient is made at random and with an equal probability, as whether to insert or extract a molecule. For this study, we perform 60% of canonical events and the 40% left for grand canonical molecule exchange. After equilibration, we perform a last run of 10^5 further MC steps per molecule to produce the average number of molecules, average energies, and all the structural analyses. The simulation box contains $(n \times m)$ orthorhombic unit cells of the substrate (i.e., $Ag_{(111)}$: 5.78 × 5.009 Å) and typically we will consider simulation boxes of (120 × 120) unit cells of the metal surface, meaning a simulation box of 693.6 × 601.08 Å for the silver surface (see Figure 2). Periodic boundary conditions are applied along the x and y directions. The simulations start from the bare surface, and we spread randomly few molecules on the substrate (e.g., <50). Adsorption isotherms allow the exploration of the accessible configurations space as a function of the incrementing chemical potential. Bruch et al. have reviewed the fundamental aspects of modeling physisorbed layers. [53] Interestingly, once a given coverage is reached, we can also perform simulations in the canonical ensemble (NVT) at a fixed number of molecules. Independently, one always sets up the maximum displacement amplitude to half of the simulation box, which insures an efficient exploration of the accessible configurations, moreover at low coverage. After 10^5 MC steps per molecule, the displacement amplitude is slowly calibrated to reach an average of 50% of successful canonical attempts, which insures an efficient equilibration. [27]

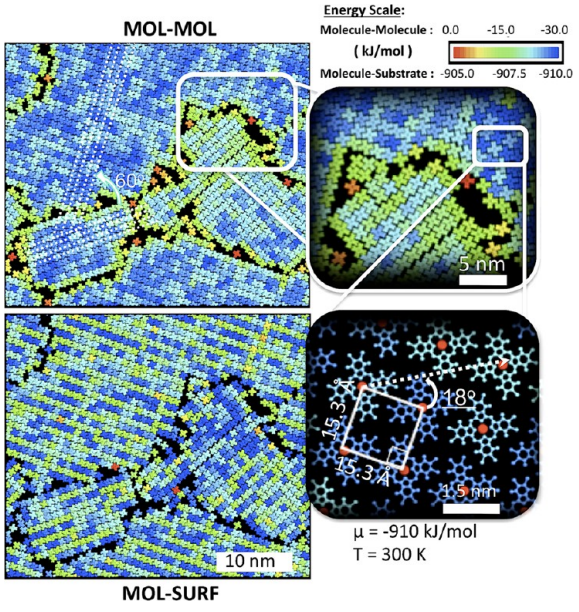

Figure 2. Snapshot of $ZnPcCl_8$ on $Ag_{(111)}$ after GCMC run at 400 K and $\mu = -910$ kJ/mol, then relaxed in NVT at 300 K. The colors scales correspond to the molecule−molecule (top left) and molecule surface (bottom left) potential energies (kJ/mol); the metal substrate is not represented. Insets represent zoomed region of the simulation box.

3. RESULTS

Phthalocyanines (Pc) molecules have a large extended π-conjugated often implying flat-lying adsorbed molecule metal surfaces. These molecules are composed of 57 atoms, and a metal is located in their center of mass, which can be substituted; by changing the nature of the metal, we can tune their optical (Zn, Cu), electronic (As, Ge), or magnetic (Fe, Co) properties. Fundamentally, these molecules are ideal systems since we can modify and enhance their adsorption potential energy on the substrate and also their intermolecular interactions by functionalizing or substituting their peripheral atoms. This latter modification can imply substrate-imposed stress on the overlayer, which can have a significant influence on the resulting molecular self-assembly.[54,55] Bellow, we first discuss the results obtained on the adsorption of octachloro-zinc-phthalocyanines molecules ($ZnPcCl_8$) on $Ag_{(111)}$ and will demonstrate the transferability of the SANO code with two other systems: the adsorption of (16-)fluoro-copper-phthalocyanines of ($CuPcF_{16}$) on $Au_{(111)}$ and PTBC on $Ag_{(111)}$.

3.1. Adsorption of $ZnPcCl_8$ Molecules on $Ag_{(111)}$. The adsorption of $ZnPcCl_8$ on $Ag_{(111)}$ metal surface has been thoroughly reported in the past decade, by means of combined experimental and ab initio theoretical studies, showing compact arrangements governed by the activation of hydrogen−chlorine bonds networks.[54] Three different phases which evolve with a relatively long time (hours) were observed experimentally:[55] first, a rhombic (P1) phase where no hydrogen bonds are formed and presumed to be stabilized by permanent dipoles localized on the chlorines when they are facing; an asymmetric (P2) phase with four eight hydrogen−chlorine bonds per molecule; and finally the most stable (P3) square phase stabilized by eight hydrogen−chlorine bonds. Experimentally,[12] the lattice parameters a and b measured for each phase are the following: P1 (lattice parameters $a_1 = b_1 = 18$ Å), intermediate phase P_2 ($a_2 = 15$ Å, $b_2 = 18$ Å), and final phase P3 ($a_3 = 15$ Å, $b_3 = 15$ Å). Another subtlety of this system is the formation of stacking faults every three rows of molecules along the $[1\bar{1}0]$ in the P3 phase, which releases the stress cumulated from the incommensurate domain formed by the point-online coincidence with the substrate.[7]

We start this study from the freestanding $ZnPcCl_8$ molecule structure reported by Oison[56] and its partial charges carried on each atom from DFT calculations. A detailed description of the nature of the hydrogen−chlorine contacts was also provided using first-principle DFT calculations. Figure 2 bellow illustrates the typical self-ordered large domain of $ZnPcCl_8$ molecules on $Ag_{(111)}$, after performing GCMC calculation at $T = 400$ K and $\mu = -910$ kJ/mol, then relaxing the equilibrated configuration at 300 K (NVT).

dx.doi.org/10.1021/ct3011248 | J. Chem. Theory Comput. 2013, 9, 2161−2169

The configuration presented in Figure 2 shows around 1700 molecules adsorbed on the silver forming large domains disoriented and following two different dense orientations of the substrate. The configuration is represented twice, colored with the intermolecular and interfacial potential energies, respectively (the bluer, the lower is the potential energy). The former tells about the defects, cluster contours, and the cumulated strain in the organic layer, while the latter reveals directly the commensurability with the substrate. In agreement with the experimental observation and DFT calculations,[56] it highlights the 'point online' coincidence[7] of the overlayer with the substrate. It means that the overlayer is orientated in a way that its two lattice vectors start and end on one class of the primitive substrate lattice lines. The closest matching supercell of the silver surface is ~14.5 per 15 Å, respectively along the $[1\bar{1}0]$ directions. The averaged overlayer square-lattice spacing presents a higher mismatch with the former direction and thus cumulates tension along it. Note that the small clusters adjust their interfacial energy to the detriment of the intermolecular interactions, which can be also directly observed on the Figure 2. We perform adsorption isotherms at different temperature close to the ambient (Figure 3).

Sharp first-order transitions in the adsorption isotherms occur at chemical potentials (μ_o^T) corresponding to the sum of the molecule−substrate potential energy (~908 kJ/mol) and the intermolecular potential energy of the first condensing clusters (from 5 to 12 kJ/mol). Importantly, the sharpness of the transition is due to the large numbers of molecules. Besides, we have experimented that small simulation boxes, leading to small amounts of molecules, bias the adsorption isotherm behavior. The effect of the temperature and the chemical potential is illustrated in the Supporting Information (Figure S1). Near the transition, large highly ordered P3 domains (i.e., several hundred of molecules per cluster) grow preferentially orientated relative to the substrate. The simulation box is filled up to 1700 molecules, reaching molecular densities around 0.37 molecules per nm^{-2}. Note that the P3 square phase has a maximum density of 0.39 molecules per nm^{-2}. The first-order transition in the adsorption isotherms is accompanied by a steep descent in the total potential energy. When extracting the different contributions to the total energy as a function of the chemical potential, one can see that the intermolecular interactions drive the ordering, leading to potential energies between 20 and 30 $kJ{\cdot}mol^{-1}$, in agreement with the binding energies reported for a square phase.[56] Also, when the temperature is raised of 100 K, the molecule−substrate potential energy increases of ~2 $kJ{\cdot}mol^{-1}$, while the intermolecular potential energy decreases of 5 $kJ{\cdot}mol^{-1}$.

To provide complementary insight into self-assembly mechanisms and the structural properties of the organic layer, we examined the size distributions of the supramolecular ordered domains along the adsorption isotherms. The different clusters were identified based on structural order criteria: the distance within a cutoff distance determined by the first $g(r)$ peak (Figure S2), the alignment between pair of first neighbor molecules and angular criterion between first common neighbors. To illustrate the effect of the temperature on the cluster sizes, we represent two configurations at 300 and 320 K, where the clusters are distinguishable by different colors and the indices give their respective number of molecules (see Figure 4). The most expanded domains reach more than a thousand of molecules. We report the average number of cluster as a function of the chemical potential and the average

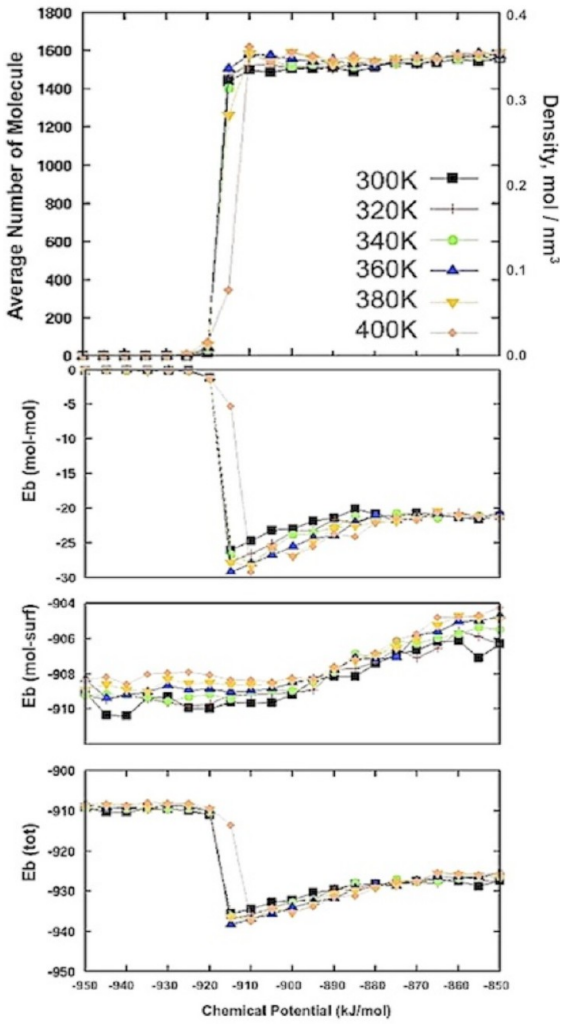

Figure 3. (top to bottom) Adsorption isotherms of $ZnPcCl_8$ on $Ag_{(111)}$ as a function of the chemical potential ($kJ{\cdot}mol^{-1}$) at six different temperatures: average number of molecules (left axis) and the corresponding molecular density ($molecules{\cdot}nm^{-2}$) follow the intermolecular, molecule−substrate, and total potential energies ($kJ{\cdot}mol^{-1}$).

cluster size distribution, which decays exponentially with the chemical potential. Interestingly, we encounter near the transition large domains with 600 molecules per cluster on average. The distribution of the average number of cluster as a function of the chemical potential follows distinguishable trends. From μ_o^T to a chemical potential of −905 kJ/mol, the average number of cluster follows a linear behavior with the presence of more than 100 molecules per cluster and <15 coexisting domains joined by either stacking faults or sharp grain boundaries. Most of them favor the $[1\bar{1}0]$ direction of the substrate. At higher chemical potential, the desorption acceptance rate decreases drastically leaving a place only for adsorption and motion MC attempts, which reduces the possibility for the molecules to reorganize and self-order. It results on a pavement of small size clusters jammed in a metastable state. Temperature annealing is then necessary to heal the organic layer.

The effects of the annealing temperature and the incrementing chemical potential on the resulting nanostructures are illustrated in Figure S1. As a general trend, the greater

dx.doi.org/10.1021/ct3011248 | J. Chem. Theory Comput. 2013, 9, 2161−2169

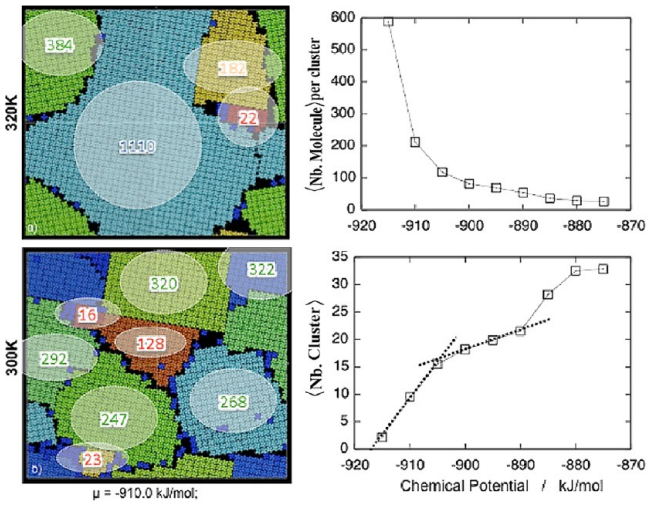

Figure 4. (left) The two structure snapshots of $ZnPcCl_8$ on $Ag_{(111)}$ at 320 K (top) and 300 K (bottom) at the same chemical potential μ = −910 kJ·mol^{-1} are colored to distinguish the different clusters, and indices show their respective number of molecules. (right) The average number of molecules per cluster (top) and the average number of clusters are plotted as a function of the chemical potential (in kJ·mol^{-1}).

the chemical potential and the lower the temperature are, the more boundaries and defects appear and the smaller are the cluster sizes. We can observe graphically the competitive alignment of each cluster along one of the three $[1\bar{1}0]$ equivalent directions of the silver (111) surface.

As a first conclusion, the GCMC approach provides good qualitative and quantitative insights on the thermodynamic and structural properties of $ZnPcCl_8$ self-ordering on $Ag_{(111)}$.

3.2. Approach Transferability. We choose two model systems to explore the transferability of the numerical approach and its capacity to retrieve the structures of two molecular building blocks with different symmetry and self-organized on two different metal surfaces. First, the adsorption of fluorinated copper-phtalocynanine ($CuPcF_{16}$) on $Au_{(111)}$ for its known ability to form a dense oblique phase. This latter molecule is of great interest when mixing it with the DIP molecule, which exhibits p- and n-type conduction properties.[28] The second system of interest is the self-assembly of PTBC adsorbed on $Ag_{(111)}$, which leads to hexagonal long-range ordered tessellations despite the C_5 symmetry of the molecule. Interestingly, Parschau et al. have reported that 2D periodic tessellations of building blocks with a five-fold molecular symmetry[57,58] to be stabilized by phase transition blocking.[59] Our interest for this molecule is also for its highly ordered phases when coadsorbed on $Ag_{(111)}$ with $ZnPcCl_8$.[60,61] Figure 5 shows two configuration snapshots during the adsorption isotherms at 300K of $CuPcF_{16}$ molecules adsorbed on $Au_{(111)}$ and PTBC molecules adsorbed on $Ag_{(111)}$.

The atomic structure of $CuPcF_{16}$ molecule and its partial charges are extracted from DFT calculations.[56] We compute the GCMC simulations at 300 K on a small simulation box of 30.6 × 26.5 nm^2. The maximum coverage reaches 0.43 molecules per nm^2. The simulation of the adsorption isotherm of $CuPcF_{16}$ molecules on Au(111) has led to an oblique molecular tilling, as illustrated in Figure 5, where the condensed phase is observed coexisting with a disordered phase. The average lattice spacing (a = 14.7 ± 0.3; b = 15.2 ± 0.3 Å and γ = 73° ± 2°) is evaluated from the radial distribution function $g(r)$ (see Figure S3), which is calculated with hundreds of configurations extracted from the last production run at equilibrium. The lattice spacing is in good agreement with the experimental arrangement (a = 14.5 ± 0.8; b = 15.1 ± 0.8 Å and γ = 75° ± 2°).[62] The intermolecular potential energy at equilibrium (−14 kJ/mol) is weaker and less directional than the $ZnPcCl_8$ chlorine-hydrogen contacts. Due to the fluorine atoms occupancy and the nature of the alkaline interactions (F−F), less accessible room is left for the molecules to adopt a closer compact arrangement, leading to the oblique phase instead of the square network observed with $ZnPcCl_8$. Interestingly, we have observed few domains with a rhombic phase coexisting with the oblique phase. Note that we have also modeled the adsorption of $CuPcF_{16}$ on copper surface and obtained the same structure, as reported experimentally.[62]

We performed adsorption isotherms of PTBC on $Ag_{(111)}$ at 300K on a simulation box of 69.41 × 60.11 nm^2, and we obtained more than 2100 molecules at high coverage, meaning approximately a molecular density of 0.5 molecules per nm^2. We observe large domains oriented independently of the $[1\bar{1}0]$ surface. Experimentally, Calmettes et al.[31] have reported the hexagonal PTBC network adsorbed on silver $Ag_{(111)}$. They have observed that PTBC networks were also orientated independently of the Ag $[1\bar{1}0]$ direction and highlighted the need for low tunneling currents in order to avoid disordered molecule motions during the tip scan, concluding that the guest molecules interact weakly with the substrate. Our calculations confirm that the interfacial potential energy (−150 kJ/mol) is much weaker than that of the metal phthalocyanines on silver and gold surfaces. Therefore, the intermolecular interactions (−27.5 kJ/mol) drive the hexagonal self-ordering, and the

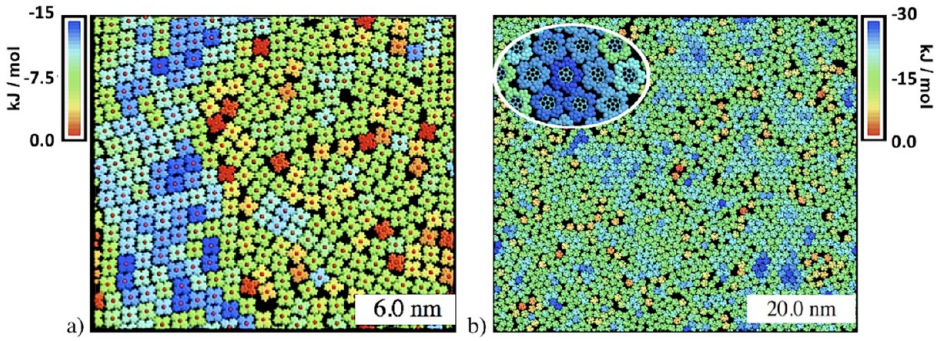

Figure 5. GCMC simulation at 300 K of (a) ∼350 $CuPcF_{16}$ molecules adsorbed on $Au_{(111)}$ and (b) ∼2100 PTBC molecules on $Ag_{(111)}$. Colors are scaled to the intermolecular potential energies.

molecular arrangements are weakly affected by the substrate. The lattice spacing of the close-compact hexagonal phase is extracted again from the $g(r)$ (see Figure S4) and is around 13.8 Å on average. Note that a shoulder in the first correlation peak arises at 13.3 Å corresponding to the most stable compact domains, in agreement with what has been measured experimentally at low temperature.

4. CONCLUSIONS

Thermodynamic properties and phase equilibrium of a supramolecular organic layer adsorbed on a surface are essential for a bottom-up device development. Typical molecular self-ordering occurs on large domains, long time scale and implies hundreds to thousands of large molecules. The SANO code overcomes the computational limitation and allows large-scale modeling spanning over the characteristic submicrometric scales. During the molecular ordering, the method confers an intuitive understanding of the subtle and competitive interplay between intermolecular and interfacial interactions. Structural properties of three model systems are successfully reproduced, leading respectively to the square, oblique, and hexagonal phases of $ZnPcCl_8$ adsorbed on $Ag_{(111)}$, $CuPcF_{16}$ on $Au_{(111)}$, and PTBC on $Au_{(111)}$.

Therefore, SANO code captures the essential physics of supramolecular self-assemblies. Taking benefits from the different generalized force fields, i.e., CHARMM and OPLS, the code is transferable and versatile. The main strength of the GCMC approach is to start the simulations from the bare surface. Therefore, one can perform readily numerical experiments starting only from the atomic structures of the molecular building blocks and the surface. Importantly, we treat thermodynamically the self-assembly at the experimental temperatures.

After this validation of the approach, the 2D (the 3D version of SANO code is under development) GCMC approach appears as a predictive numerical tool. The code is also extended to multicomponent self-assembly. A large scope of physical properties becomes accessible as a function of the coverage, for instance, the effect of the substrate roughness on the long-range molecular order; the cumulative stress on the organic layer due to the heteroepitaxy; the commensurability for a given molecular superstructure; and phase equilibrium of bimolecular systems as a function of the relative concentration. Ultimately, the method is versatile and can be an interesting multiscale approach if one aims to bridge quantum level calculations to the experimental scale and within a treatment in temperature.

■ ASSOCIATED CONTENT

Supporting Information

Annealing temperature and chemical potential effects on the $ZnPcCl_8$ molecular ordering on $Ag_{(111)}$ surface; the standard structural analysis (e.g., radial distribution function and intermolecular angular distribution) used to extract the average angular and lattice spacing of the different structures; and references for the parameters implemented in the SANO code. This information is available free of charge via the Internet at http://pubs.acs.org

■ AUTHOR INFORMATION

Corresponding Author

*E-mail: troussel@icmab.es

Notes

The authors declare no competing financial interest.

■ ACKNOWLEDGMENTS

T.R. is supported by a JAEdoc contract cofunded by CSIC and the European Union funds. T.R. thanks the Ministerio de Ciencia for financial support through projects FIS2009-13370-C02-02 and CONSOLIDER-NANOSELECT-CSD2007-00041. We also acknowledge the CESGA Supercomputing Center for computational time and technical assistance. T.R. deeply acknowledges Dr. Jordi Faraudo for its helpful discussions. This work has been partially financed by the Spanish government, Ministerio de Ciencia e Innovacion, under projects CTQ2008-05370/PPQ, and by the Catalan Government under project SGR2009-666. Additional support from Carburos Metallicos, Air Products Group, is also acknowledged.

■ REFERENCES

(1) Barth, J. V.; Costantini, G.; Kern, K. Engineering atomic and molecular nanostructures at surfaces. *Nature* **2005**, *437*, 671−679.

(2) Barth, J. V. Molecular Architectonic on Metal Surfaces. *Annu. Rev. Phys. Chem.* **2007**, *58*, 375−407.

(3) Oteyza, D.; Barrena, E.; Dosch, H.; Ortega, J. E.; Wakayama, Y. Tunable symmetry and periodicity in binary supramolecular nanostructures. *Phys. Chem. Chem. Phys.* **2011**, *13*, 4220−4223.

(4) Neel, N.; Krögerand, J.; Berndt, R. Highly Periodic Fullerene Nanomesh. *Adv. Mater.* **2006**, *18*, 174−177.

(5) Oteyza, D.; Barrena, E.; Ruiz-Oses, M.; Silanes, I.; Doyle, B. P.; Ortega, J. E.; Arnau, A.; Dosch, H.; Wakayama, Y. Crystallographic and Electronic Structure of Self-Assembled DIP Monolayers on Au(111) Substrates. *J. Phys. Chem. C* **2008**, *112*, 7168−7172.

(6) Sun, X.; Jonkman, H. T.; Silly, F. Tailoring two-dimensional PTCDA−melamine self-assembled architectures at room temperature by tuning molecular ratio. *Nanotechnology* **2010**, *21* (16), 165602.

(7) Hooks, D. E.; Fritz, T.; Ward, M. D. Epitaxy and molecular organization on solid substrates. *Adv. Mater.* **2001**, *13* (4), 227−241.

(8) Kühnle, A. Self-assembly of organic molecules at metal surfaces. *Curr. Opin. Colloid Interface Sci.* **2009**, *14*, 157−168.

(9) Bauert, T.; Zoppi, L.; Koller, G.; Garcia, A.; Baldridge, K. K.; Ernst, K.-H. Large Induced Interface Dipole Moments without Charge Transfer: Buckybowls on Metal Surfaces. *J. Phys. Chem. Lett.* **2011**, *2*, 2805−2809.

(10) Seitsonen, A. P.; Lingenfelder, M.; Spillmann, H.; Dmitriev, A.; Stepanow, S.; Lin, N.; Kern, K.; Barth, J. V. Density Functional Theory Analysis of Carboxylate-Bridged Diiron Units in Two-Dimensional Metal-Organic Grids. *J. Am. Chem. Soc.* **2006**, *128*, 5634−5635.

(11) Saiz-Poseu, J.; Martínez-Otero, A.; Roussel, T.; Hui, J.K.-H; Montero, M. L.; Urcuyo, R.; MacLachlan, M. J.; Faraudo, J.; Ruiz-Molina, D. Self-assembly of a catechol-based macrocycle at the liquid−solid interface: experiments and molecular dynamics simulations. *Phys. Chem. Chem. Phys.* **2012**, *14* (34), 11937−11943.

(12) Koudia, M.; Abel, M.; Maurel, C.; Bliek, A.; Catalin, D.; Mossoyan, M.; Mossoyan, J.-C.; Porte, L. Influence of Chlorine Substitution on the Self-Assembly of Zinc Phthalocyanine. *J. Phys. Chem. B* **2006**, *110*, 10058−10062.

(13) Misiunas, T.; Tornau, E. E. Ordered Assemblies of Triangular-Shaped Molecules with Strongly Interacting Vertices: Phase Diagrams for Honeycomb and Zigzag Structures on Triangular Lattice. *J. Phys. Chem. B* **2012**, *116*, 2472−2482.

(14) Weber, U. K.; Burlakov, V. M.; Perdigãao, L. M. A.; Fawcett, R. H. J.; Beton, P. H.; Champness, N. R.; Jefferson, J. H.; Briggs, G. A. D.; Pettifor, D. G. Role of Interaction Anisotropy in the Formation and Stability of Molecular Templates. *Phys. Rev. Lett.* **2008**, *100*, 156101.

(15) Silly, F.; Weber, U. K.; Shaw, A. Q.; Burlakov, V. M.; Castell, M. R.; Briggs, G. A. D.; Pettifor, D. G. Deriving molecular bonding from a macromolecular self-assembly using kinetic Monte Carlo simulations. *Phys. Rev. B* **2008**, *77*, 201408(R).

(16) Patti, A.; Ramsch, R.; MarsaMarsà, C. S. Solvent-Free Model for Self-Assembling Amphiphilic Cyclodextrins. An Off-Lattice Monte Carlo Approach in Two Dimensions. *J. Phys. Chem. B* **2012**, *116*, 2687−2695.
(17) Fortuna, S.; Troisi, A. An Artificial Intelligence Approach for Modeling Molecular Self-assembly: Agent-based Simulations of Rigid Molecules. *J. Phys. Chem. B* **2009**, *113*, 9877−9885.
(18) Fortuna, S.; Troisi, A. Agent-Based Modeling for the 2D Molecular Self-Organization of Realistic Molecules. *J. Phys. Chem. B* **2010**, *114*, 10151−10159.
(19) Martsinovich, N.; Troisi, A. Modeling the Self-Assembly of Benzenedicarboxylic Acids Using Monte Carlo and Molecular Dynamics Simulations. *J. Phys. Chem. C* **2010**, *114*, 4376−4388.
(20) Pannetier, J.; Bassas-Alsina, J.; Rodriguez-Carvajal, J.; Caignaert, V. Prediction of crystal structures from crystal chemistry rules by simulated annealing. *Nature* **1990**, *346*, 343−345.
(21) Builes, S.; Roussel, T.; Vega, L. F. Optimization of the Separation of Sulfur Hexafluoride and Nitrogen by Selective Adsorption Using Monte Carlo Simulations. *AIChE J.* **2011**, *57*, 962−974.
(22) Builes, S.; Roussel, T.; Matei Ghimbeu, C.; Parmentier, J.; Gadiou, R.; Vix-Guterl, C.; Vega, L. F. Microporous carbon adsorbents with high CO2 capacities for industrial applications. *Phys. Chem. Chem. Phys.* **2011**, *13*, 16063−16070.
(23) Roussel, T.; Didion, A.; Pellenq, R.J.-M.; Gadiou, R.; Bichara, C.; Vix-Guterl, C. Experimental and Atomistic Simulation Study of the Structural and Adsorption Properties of Faujasite Zeolite-Templated Nanostructured Carbon Materials. *J. Phys. Chem. C* **2007**, *111*, 15863−15816.
(24) Kirkpatrick, S.; Gelatt, C. D.; Vecchi, M. P. Optimization by Simulated Annealing. *Science* **1983**, *220* (4598), 671−680.
(25) Mannsfeld, C. B. *Ph.D. Thesis*. Staats und Universitatsbibliothek Dresden, Dresden, Germany, 2004.
(26) Mannsfeld, S. C. B.; Fritz, T. Advanced Modelling of Epitaxial Ordering of Organic Layers on Crystalline Surface. *Mod. Phys. Lett. B* **2006**, *20* (11), 585−605.
(27) Frenkel, D.; and Smit, B. *Understanding Molecular Simulation: From Algorithms to Applications*; Academic Press: San Diego, 2002.
(28) Barrena, E.; Oteyza, D.; Dosch, H.; Wakayama, Y. 2D Supramolecular Self-Assembly of Binary Organic Monolayers. *Chem. Phys. Chem.* **2007**, *8*, 1915−1918.
(29) Oteyza, D.; Barrena, E.; Dosch, H.; Ortega, J. E.; Wakayama, Y. Tunable symmetry and periodicity in binary supramolecular nanostructures. *Phys. Chem. Chem. Phys.* **2011**, *13*, 4220−4223.
(30) Oteyza, D. G.; El-Sayed, A.; Garcia-Lastra, J. M.; Goiri, E.; Krauss, T. N.; Turak, A.; Barrena, E.; Dosch, H.; Zegenhagen, J.; Rubio, A.; Wakayama, Y.; Ortega1, J. E. Copper-phthalocyanine based metal−organic interfaces: The effect of fluorination, the substrate, and its symmetry. *J. Chem. Phys.* **2010**, *133*, 214703.
(31) Calmettes, B.; Nagarajan, S.; Gourdon, A.; Benjalal, Y.; Bouju, X.; Abel, M.; Porte, L.; Coratger, R. Properties of Penta-tert-butylcorannulene Molecules Inserted in Phthalocyanine Networks Studied by Low-Temperature Scanning Tunneling Microscopy. *J. Phys. Chem. C* **2009**, *113*, 21169−21176.
(32) Mannsfeld, S. C. B.; Fritz, T. Understanding organic−inorganic heteroepitaxial growth of molecules on crystalline substrates: Experiment and theory. *Phys. Rev. B* **2005**, *71* (23), 235405.
(33) *HyperChem Computational Chemistry*; Hypercube, Inc.: Gainesville, FL, 1996.
(34) Soler, J. M.; Artacho, E.; Gale, J. D.; García, A.; Junquera, J.; Ordejón, P.; Sánchez-Portal, D. The Siesta method for ab initio order-N materials simulation. *J. Phys.: Condens. Matter* **2002**, *14*, 2745−2779.
(35) Bardeen, J. The image and van-der-Waals forces at a metallic surface. *Phys. Rev.* **1940**, *58*, 727−736.
(36) Lang, N. D.; Kohn, W. Theory of metal surfaces: induced surface charge and image potential. *Phys. Rev. B* **1973**, *7*, 3541−3550.
(37) Heinz, H.; Jha, K. C.; Luettmer-Strathmann, J.; Farmer, B. L.; Naik, R. R. Polarization at metal−biomolecular interfaces in solution. *J. R. Soc. Interface* **2011**, *8*, 220−232.
(38) Heinz, H.; Vaia, R. A.; Farmer, B. L.; Naik, R. R. Accurate Simulation of surfaces and interfaces of face-centered cubic metals using 12−6 and 9−6 Lennard-Jones potentials. *J. Phys. Chem. C* **2008**, *112*, 17281.
(39) Feng, J.; Pandey, R. B.; Berry, R. J.; Farmer, B. L.; Naik, R. R.; Heinz, H. Adsorption mechanism of single amino acid and surfactant molecules to Au {111} surfaces in aqueous solution: design rules for metal-binding molecules. *Soft Matter* **2011**, *7*, 2113−2120.
(40) Jorgensen, W. L.; Maxwell, D. S.; Tirado-Rives, J. Development and Testing of the OPLS All-Atom Force Field on Conformational Energetics and Properties of Organic Liquids. *J. Am. Chem. Soc.* **1996**, *118*, 11225.
(41) Chulkov, E. V.; Silkin, V. M.; Echenique, P. M. Image potential states on metal surfaces: binding energies and wave functions. *Surf. Sci.* **1999**, *437*, 330−352.
(42) Mehl, M. J.; Papaconstantopoulos, D. A. Applications of a tight-binding total-energy method for transition and noble metals: Elastic constants, vacancies, and surfaces of monatomic metals. *Phys. Rev. B* **1996**, *54*, 4519−4530.
(43) MacKerell, A. D., Jr.; Feig, M.; Brooks, C. L., III. Extending the treatment of backbone energetics in protein force fields: limitations of gas-phase quantum mechanics in reproducing protein conformational distributions in molecular dynamics simulations. *J. Comput. Chem.* **2004**, *25*, 1400−1415.
(44) Mottet, C.; Tréglia, G.; Legrand, B. Structures of a Ag monolayer deposited on Cu(111), Cu(100) and Cu(110) substrates: an extended tight-binding quenched-molecular-dynamics study. *Phys. Rev. B* **1992**, *46* (24), 16018−16030.
(45) Ducastelle, F. Modules élastiques des métaux de transition. *J. Phys. (Paris)* **1970**, *31*, 1055.
(46) Rosato, V.; Guillope, M.; Legrand, B. Thermodynamical and structural properties of f.c.c. transition metals using a simple tight-binding model. *Philos. Mag. A* **1989**, *59*, 321−336.
(47) Gupta, R. P. Lattice relaxation at a metal surface. *Phys. Rev. B* **1981**, *23*, 6265−6270.
(48) Mottet, C.; Tréglia, G.; Legrand, B. Structures of a Ag monolayer deposited on Cu(111), Cu(100) and Cu(110) substrates: an extended tight-binding quenched-molecular-dynamics study. *Phys. Rev. B* **1992**, *46* (24), 16018−16030.
(49) Ouahab, A.; Mottet, C.; Goniakowski, J. Atomistic simulation of Ag thin films on MgO(100) substrate: A template substrate for heterogeneous adsorption. *Phys. Rev. B* **2005**, *72* (03), 035421.
(50) Goniakowski, J.; Mottet, C. Simulation of the growth of metal nanoclusters on the MgO(100) surface. *Phys. Rev. B* **2010**, *81* (15), 155443.
(51) Goyhenex, C. Revised tight-binding second moment potential for transition metal surfaces. *Surf. Sci.* **2012**, *606*, 325−328.
(52) Nicholson, D.; and Parsonage, N. G.; In Computer Simulation and the Statistical Mechanics of Adsorption; Academic Press: London, 1982.
(53) Bruch, L. W.; Diehl, R. D.; Venables, J. A. Progress in the measurement and modeling of physisorbed layers. *Rev. Mod. Phys.* **2007**, *79* (4), 1381−1454.
(54) Oison, V.; Koudia, M.; Abel, M.; Porte, L. Influence of stress on hydrogen-bond formation in a halogenated phthalocyanine network. *Phys. Rev. B* **2007**, *75* (3), 035428.
(55) Milde, P.; Zerweck, U.; Eng, L.; Abel, M.; Giovanelli, L.; Nony, L.; Mossoyan, M.; Porte, L.; Loppacher, Ch. Interface dipole formation of different ZnPcCl8 phases on Ag(111) observed by Kelvin probe force microscopy. *Nanotechnology* **2008**, *19* (30), 305501.
(56) Oison, V. First-principle study of the hydrogen bonds in a thin film of phthalocyanine molecules. *Surf. Sci.* **2007**, *601*, 1040−1047.
(57) Parschau, M.; Fasel, R.; Ernst, K.-H.; Greoning, O.; Brandenberger, L.; Schillinger, R.; Greber, T.; Seitsonen, A.; Wu, Y.-T.; Siegel, J. S. Buckybowls on Metal Surfaces: Symmetry Mismatch and Enantiomorphism of Corannulene on Cu(110). *Angew. Chem., Int. Ed.* **2007**, *46*, 8258−8261.

(58) Merz, L.; Parschau, M.; Zoppi, L.; Baldridge, K. K.; Siegel, J. S.; Ernst, K.-H. Reversible Phase Transitions in a Buckybowl Monolayer. *Angew. Chem., Int. Ed.* **2009**, *48*, 1966−1969.
(59) Merz, L.; Bauert, T.; Parschau, M.; Koller, G.; Siegel, J. S.; Ernst, K.-H. Polymorph selection in 2D crystals by phase transition blocking. *Chem. Commun.* **2009**, *39*, 5871−5873.
(60) Guillermet, O.; Niemi, E.; Nagarajan, S.; Bouju, X.; Martrou, D.; Gourdon, A.; Gauthier, S. Self-Assembly of Fivefold-Symmetric Molecules on a Threefold-Symmetric Surface. *Angew. Chem., Int. Ed.* **2009**, *48*, 1970−1973.
(61) Calmettes, B.; Nagarajan, S.; Gourdon, A.; Abel, M.; Porte, L.; Coratger, R. Bicomponent Supramolecular Packing in Flexible Phthalocyanine Networks. *Angew. Chem., Int. Ed.* **2008**, *47*, 6994−6998.
(62) Oteyza, D.; Silanes, I.; Ruiz-Oses, M.; Barrena, E.; Doyle, B. P.; Arnau, A.; Dosch, H.; Wakayama, Y.; Ortega, J. E. Balancing Intermolecular and Molecule−Substrate Interactions in Supramolecular Assemblies. *Adv. Funct. Mater.* **2009**, *19*, 259−264.